Terahertz radiation induces non-thermal structural changes associated with Fröhlich condensation in a protein crystal

Ida V. Lundholm,[1,a)] Helena Rodilla,[2,a)] Weixiao Y. Wahlgren,[1] Annette Duelli,[1] Gleb Bourenkov,[3] Josip Vukusic,[2] Ran Friedman,[4] Jan Stake,[2] Thomas Schneider,[3] and Gergely Katona[1,b)]

[1]*Department of Chemistry and Molecular Biology, University of Gothenburg, Gothenburg, Sweden*
[2]*Department of Microtechnology and Nanoscience, Chalmers University of Technology, Gothenburg, Sweden*
[3]*European Molecular Biology Laboratory Hamburg Outstation, EMBL c/o DESY, Notkestrasse 85, 22603 Hamburg, Germany*
[4]*Department of Chemistry and Biomedicinal Sciences and Centre for Biomaterials Chemistry, Linnaeus University, Kalmar, Sweden*

(Received 9 July 2015; accepted 14 September 2015; published online 13 October 2015)

Whether long-range quantum coherent states could exist in biological systems, and beyond low-temperature regimes where quantum physics is known to be applicable, has been the subject to debate for decades. It was proposed by Fröhlich that vibrational modes within protein molecules can order and condense into a lowest-frequency vibrational mode in a process similar to Bose-Einstein condensation, and thus that macroscopic coherence could potentially be observed in biological systems. Despite the prediction of these so-called Fröhlich condensates almost five decades ago, experimental evidence thereof has been lacking. Here, we present the first experimental observation of Fröhlich condensation in a protein structure. To that end, and to overcome the challenges associated with probing low-frequency molecular vibrations in proteins (which has hampered understanding of their role in proteins' function), we combined terahertz techniques with a highly sensitive X-ray crystallographic method to visualize low-frequency vibrational modes in the protein structure of hen-egg white lysozyme. We found that 0.4 THz electromagnetic radiation induces non-thermal changes in electron density. In particular, we observed a local increase of electron density in a long α-helix motif consistent with a subtle longitudinal compression of the helix. These observed electron density changes occur at a low absorption rate indicating that thermalization of terahertz photons happens on a micro- to milli-second time scale, which is much slower than the expected nanosecond time scale due to damping of delocalized low frequency vibrations. Our analyses show that the micro- to milli-second lifetime of the vibration can only be explained by Fröhlich condensation, a phenomenon predicted almost half a century ago, yet never experimentally confirmed. [http://dx.doi.org/10.1063/1.4931825]

INTRODUCTION

Understanding molecular vibrations in proteins is important because they regulate the function of proteins, e.g., in enzyme catalysis and protein interactions. In particular, low-frequency collective vibrational modes of proteins in the terahertz frequency region

[a)]I. V. Lundholm and H. Rodilla contributed equally to this work.
[b)]Author to whom correspondence should be addressed. Electronic mail: gergely.katona@cmb.gu.se

(0.1–10 THz) are expected to have a strong influence on protein function, for example, in the enzyme adenylate kinase picosecond (ps) vibrations are involved in the opening of the active site "lid."[1–3] But understanding low-frequency vibrational modes in proteins is difficult for two reasons. First, probing vibrational modes in proteins requires detailed analyses of absorption spectra. While high-frequency molecular vibrations, where only a few atoms are involved, can be identified and associated with well-resolved peaks in absorption spectra obtained using mid-infrared or Raman spectroscopy, slower collective vibrations in the terahertz regime are difficult to identify because more atoms are involved in the absorption process and the absorption also depends on the three-dimensional arrangement of the polypeptide chain (protein fold)—these factors, combined, lead to poorly resolved spectra with substantial spectral line broadening.

Second, once terahertz radiation is absorbed by proteins, there are widely different speculations about the fate of the excited state. According to one model, the absorption of THz photons gives rise to delocalized molecular vibrations that are quickly ($<$1 ns) damped, with the energy thereby being dissipated to the environment in the form of thermal energy (thermalization).[4,5] In contrast, in 1968 Fröhlich offered a radically different hypothetical model,[6] frequently referred to as Fröhlich condensation, whereby not all energy supplied to the protein is directly thermalized. Instead, according to Fröhlich's hypothetical model, the protein could be described as a group of coupled oscillators (in a thermal bath), which could condense into the lowest-frequency-mode when energy is supplied to the system, in a process similar to Bose-Einstein condensation.

A considerable amount of theoretical and experimental work has been done in the past in order to demonstrate the influence of THz radiation in biological systems with no clear results due to the complexity of the required experiments.[7] Here we report the, to our knowledge first, experimental observation of Fröhlich condensation in a biological system. To that end, we used X-ray crystallography combined with THz radiation to visualize structural changes associated with low-frequency collective vibrations induced in lysozyme protein crystals by irradiation with 0.4 THz radiation and detected steady state structural changes that are sustained for micro- to milli-seconds, which is 3–6 orders of magnitude longer than expected if the structural changes would be due to a redistribution of vibrations upon terahertz absorption following Boltzmann's distribution. Our analyses show that the long lifetime of these structural changes can only be explained by Fröhlich condensation. Our results thus provide the first strong evidence for the occurrence of Fröhlich condensation in a protein structural network and indicate that macroscopic quantum effects may manifest in biological systems.

RESULTS AND DISCUSSION

The lysozyme protein system

We chose lysozyme as a model system because (1) previous studies have indicated that low-frequency vibrations strongly influence the protein's functional state and it is thus important to probe these and (2) it is a promising test-bed for observing Fröhlich condensation. Lysozyme is a hydrolytic enzyme that is part of the immune system of all multicellular eukaryotes. It acts as the first line of defense against a bacterial infection by hydrolyzing parts of the bacterial cell wall which leads to cell lysis. It is mainly composed of an alpha helical secondary structure and each alpha helix is a macro dipole. The presence of macro dipoles makes lysozyme a good candidate to test the Fröhlich model because it has been shown that polar characteristics are required for the condensate to form.[8] It has also been shown that the terahertz spectrum of lysozyme changes upon inhibitor binding,[5] indicating an important connection between low frequency vibrations and the functional state of the protein. Furthermore, molecular vibrations have also been shown to play a key role in the catalytic mechanism of lysozyme.[9]

X-ray diffraction visualization of protein structure changes induced by THz radiation

To visualize the structural changes induced in the lysozyme crystal structure by THz radiation we measured the X-ray diffraction of lysozyme crystals during alternating 25 ms on and off states (50% duty cycle) of a terahertz source at 0.4 THz. The diffraction data was then separated into two groups (terahertz on and terahertz off) and processed separately yielding two separate sets of scaled and merged reflections (the data quality of this data collection strategy is evaluated in the supplementary material and Table S1).[10] The alternating on and off terahertz illumination, together with a very small (0.01°) crystal rotation per frame, made it possible to acquire both ground state (from the terahertz off group) and terahertz excited state (from the terahertz on group) from the same crystal. When collecting X-ray diffraction data of a protein crystal, there are several factors that can affect the quality of the data. The major factor is X-ray radiation inflicted damage on the crystal that causes a loss in diffraction intensity over time thereby introducing uncertainty in the atomic positions in the structural model. Different crystals also diffract differently due to mosaicity and crystal size. Thus, employing the method described here, changes in diffraction due to crystal differences are avoided and the difference in X-ray dose will be significantly reduced.

Diffraction data were recorded from seven crystals on 142 500 diffraction frames in total for all crystals. The merged diffraction data and refinement statistics are summarized in Table I. A control experiment was also performed to ensure that any effect arising is induced by terahertz illumination and not due to the data collection strategy itself or any other unknown factor. The control experiment data was collected by measuring diffraction on consecutive images with no illumination and grouping them in two separate data sets determined by the parity of the image sequence number (odd and even). Merged diffraction data and refinement statistics for the control experiment are summarized in Table S2.[10]

TABLE I. Crystal and structure refinement data for terahertz illuminated crystals.

	THz on	THz off
Data collection		
Space group	$P4_32_12$	$P4_32_12$
Cell dimensions		
a and b (Å)	79.4	79.4
c (Å)	37.4	37.4
α, β, and γ (deg)	90, 90, 90	90, 90, 90
Resolution (Å)	15.0–1.7	15.0–1.7
R_{merge} (%)[a,b]	9.4 (74.0)	9.4 (76.3)
$CC_{1/2}$[a]	100.0 (99.1)	100.0 (99.1)
$\langle I/\sigma(I)\rangle$[a]	75.6 (10.5)	75.6 (10.1)
Completeness (%)	91.1 (66.7)	90.9 (65.2)
Redundancy	197.0	197.0
Refinement		
No. reflections	11 830	11 829
R_{work}/R_{free} (%)[c]	16.6/19.1	16.6/19.0
No. atoms (protein)	1042	1042
r.m.s. deviations		
Bond lengths (Å)	0.0229	0.0229
Bond angles (deg)	1.9907	1.9804

[a]Values for the highest resolution shell (1.70–1.74 Å) are shown in parentheses.
[b]$R_{merge} = \sum_h\sum_i|I(h)_i - \langle I(h)\rangle|/\sum_h\sum_i|I(h)_i|$, where $I(h)_i$ is the **i**th intensity measurement of a reflection and I(h) the average intensity from multiple reflections.
[c]R-factor $= \sum|F_o - F_c|/\sum F_o$.

To identify the changes in electron density in the protein crystal induced by terahertz irradiation we calculated a difference electron density map between terahertz on and off states, $F_{0.4THz} - F_{off}$ (Fig. 1). The most striking feature of the electron density map is four positive peaks (electron density increase upon terahertz illumination) that are clustered around helix 3 (amino acid residues 86–101) that forms the substrate binding cleft (the backbone ribbon model of the entire structure is shown in Fig. 1(a) and the atomic model of helix3 in Fig. 1(b)). Four of the six strongest differences in Fourier peaks are located in the region around helix 3 (Table S3).[10] An induced structural change in helix 3 is possible since its movement is unhindered by crystal contacts. The significant electron density changes in the map are not caused by noise since they are non-uniformly distributed. Validation of the $F_{0.4THz} - F_{off}$ difference in electron density map to ensure that the observed electron density features persist after resampling the diffraction data is described in the supplementary material and Fig. S1.[10] No significant

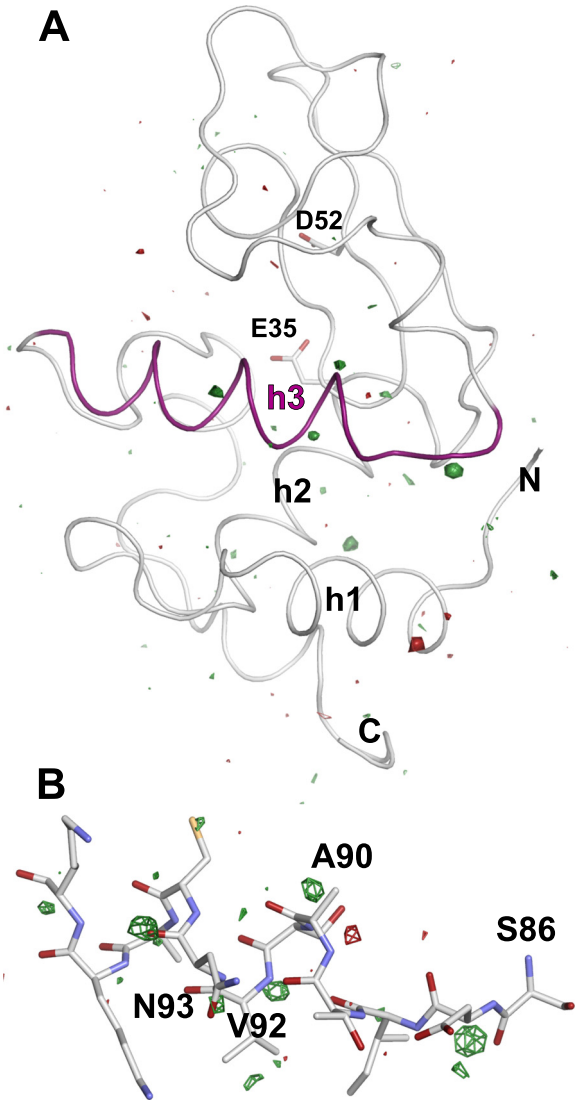

FIG. 1. Difference-Fourier maps ($F_{0.4THz} - F_{off}$) showing the changes in electron density induced by exposing a lysozyme protein crystal to 0.4 THz radiation. The entire structure is shown in (a) with helix 3 highlighted in red, the N and C-terminus of the polypeptide chain is marked together with the three helices present in the structure (h1, h2, and h3). The active site residues E35 and D52 are marked. (b) Zoom in of helix 3 with the positive difference electron density peaks. The contour level of the map in (a) is 3.4 σ (5.5 $me^{-}/Å^3$) and in (b) 2.8 σ. Green and red color indicate increased and decreased electron density upon terahertz illumination, respectively.

differences close to any structural elements can be observed in the control difference Fourier electron density map between odd and even frames (Fig. S2).[10]

Structural analysis

To understand how the observed electron-density-increase caused by terahertz radiation is linked to corresponding structural changes in the protein crystal we investigated changes in model parameters such as atomic positions and B-factors (factor describing atomic displacement) between lysozyme structural models based on $\langle F_{0.4THz}\rangle$ and $\langle F_{off}\rangle$ data sets derived from the 0.4 THz experiment and the $\langle F_{odd}\rangle$ and $\langle F_{even}\rangle$ data sets derived from the control experiment. The difference between model parameters based on the $\langle F_{0.4THz}\rangle$ and $\langle F_{off}\rangle$ data ($M_{0.4THz} - M_{off}$) and the difference between model parameters based on the $\langle F_{odd}\rangle$ and $\langle F_{even}\rangle$ data ($M_{odd} - M_{even}$) were calculated.

From the obtained different models, $M_{0.4THz} - M_{off}$ and $M_{odd} - M_{even}$, the difference in atomic positions was projected onto the longitudinal axis of helix 3 (Fig. 2) and we found that terahertz radiation induces positional shifts in several atoms, for example, in Cβ of Ala-90, which is also close to one of the positive electron density peaks from the difference map (Fig. 1(b)). Overall, the terahertz radiation was found to result in a compression of the helix (Fig. 2(b)).

As a next step, we analysed the B-factors given by the models, $M_{0.4THz} - M_{off}$ and $M_{odd} - M_{even}$. The $M_{odd} - M_{even}$ B-factor difference is mainly positive for all residues (Fig. 3). This is due to the higher X-ray dose for even frames compared to odd frames consequence of the 25 ms extra X-ray exposure (5.5 Gy) that the even frames received compared to the odd frames due to the recording sequence. On the other hand, the $M_{0.4THz} - M_{off}$ B-factor differences

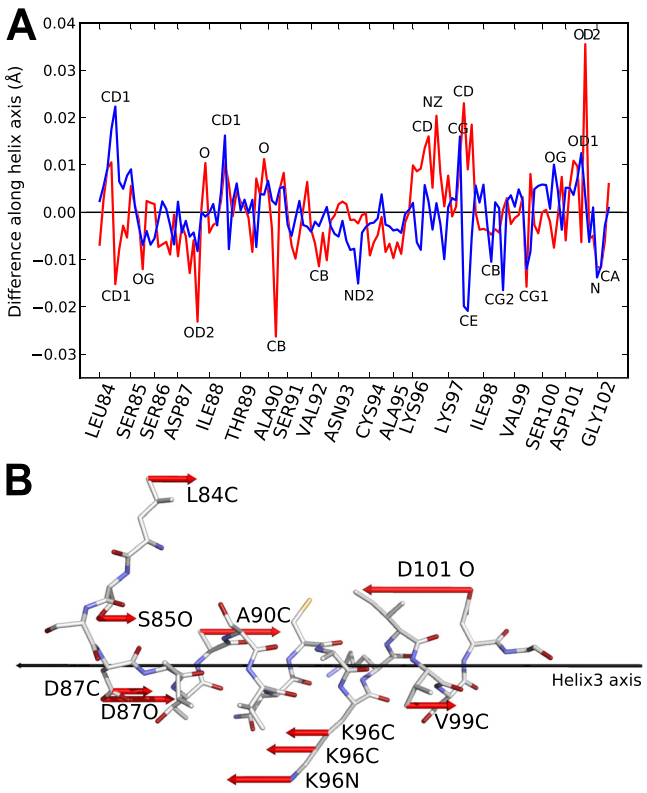

FIG. 2. Change in atomic positions in the lysozyme protein structure in response to terahertz radiation, projected onto the longitudinal axis of helix 3. (a) Projected atomic coordinate differences between crystallographic model refined against 0.4 THz illuminated frames and THz off frames (red) and coordinate differences for models refined against odd and even frames of the reference data (blue). (b) The direction and relative amplitude of the largest coordinate changes upon 0.4 THz illumination shown as red arrows drawn on a full atom structural model of helix3.

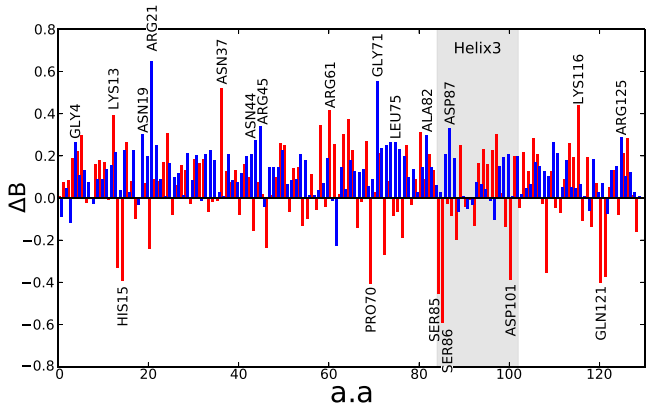

FIG. 3. B-factor difference plots. B-factor differences between crystallographic model refined against 0.4 THz illuminated frames and THz off frames (red) and difference in average B-factors per residue for models refined against odd and even frames of the reference data (blue). The residues of helix 3 are highlighted with the grey box.

display both negative and positive differences (Fig. 3), despite the same X-ray dose difference as for the $M_{odd} - M_{even}$ difference model. The B-factor is a measure of atomic displacement, hence a lower B-factor is related to a more ordered system. Since the $M_{odd} - M_{even}$ model gives more positive B-factor differences than the $M_{0.4THz} - M_{off}$ model, we draw the conclusion that terahertz radiation cause atoms to become more ordered in comparison with the ground state. Notably, the residues Ser86 and Asp101 of the protein structure irradiated with terahertz radiation have a lower B-factor compared to the non-irradiated sample (Fig. 3) and are both situated close to the position for which we observed the positive electron density features (Fig. 1(b)). The observed combination of compression of the helix 3 and increased atomic order induced by terahertz radiation lead to electrons being confined in a volume that is smaller than the one occupied by electrons in the ground state, which in turn gives rise to the observed positive electron density difference.

Structural changes are not caused by heating

Our measurements reveal that terahertz radiation gives rise to structural changes in the protein crystal structure, but could these changes be a consequence of heating induced by the radiation? As our following analysis will show, the answer is negative because of the following reasons: First, random vibrations induced by heating should lead to an expansion of helix 3 and less atomic order, which is counter to our observation of a compression of helix 3 and increased ordering in the atomic positions.

Second, to eliminate the possibility that an increase in temperature could cause a shift in either the chemical or conformational equilibrium, we measured the heating profile of a lysozyme crystal under 0.4 THz illumination with a thermal camera. From this measurement, we estimated that 20 ms illumination with terahertz radiation (which was the recording time of each diffraction frame in our experiment) results in an average temperature increase of 1 mK (details of the heating estimations can be found in the "Materials and Methods" section). This estimated temperature increase would increase the average kinetic energy of the crystal by 86 neV, which is six orders of magnitude smaller than the 26 meV kinetic energy (kT) at 297 K (the temperature of the sample during data collection).

This 1 mK temperature increase would shift the conformational state population by at most 0.1%. We obtained this estimate by relating the temperature increase to a change in equilibrium constant of a conformational state population (described by the van't Hoff equation) via enthalpy. We can look at what 1 mK temperature increase does in the most widely studied conformational change of proteins: thermal unfolding. Proteins of the size of lysozyme have an unfolding enthalpy of approximately 500 kJ/mol.[11] The point in the unfolding process where the conformational state equilibrium is most affected by temperature is close to the melting

temperature (where the population of folded and unfolded state is equal). Even if we consider this implausible case (large enthalpy change and system exactly at melting temperature), a 1 mK temperature increase would only shift the conformational state population by 0.1%. In the folded state of the protein, conformational changes likely have much smaller associated changes in enthalpy, and thus, a smaller potential shift in conformational equilibrium. If only the classical thermodynamic principles are concerned, at this power of terahertz radiation, the induced temperature change is too small to influence a conformational equilibrium in a measurable way and cannot explain the observed electron density changes.

Structural changes are attributed to Fröhlich condensation

If heating is not causing the observed structural changes induced by terahertz radiation, what is the origin of the changes in the protein crystal structure? We argue that the observed structural changes are caused by the formation of a Fröhlich condensate that generates a new state of the protein that is compatible with the observed helix compression.

To provide evidence for the existence of a Fröhlich condensate in our protein structure, we performed normal mode analysis on a structural model of lysozyme. Fröhlich condensation would lead to a redistribution of energy into one vibrational mode from an ensemble of occupied modes present in the ground state. This can occur even for relatively small-amplitude harmonic vibrations. To illustrate this, in the inset of Fig. 4(a), we show the overlap of the atomic positions during motions of ten selected normal modes affecting residues T89 and A90 of helix 3. If illumination of lysozyme with 0.4 THz would cause energy redistribution into one of the vibrational modes, according to Fröhlich theory, that mode would dominate the atomic motion. Consequently, in the following analysis we explored all ten possible configurations where the excited state is represented by only one mode, and the ground state is represented by an

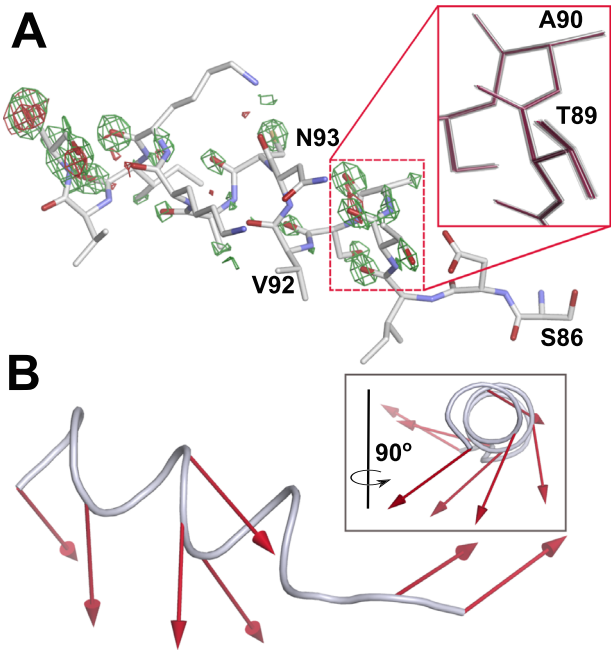

FIG. 4. Normal mode analysis and theoretical electron density maps. (a) Difference Fourier map calculated between structure factor amplitudes derived from models with different occupancies of normal modes to represent the terahertz excited state and the ground state. The terahertz excited state model was represented with one normal mode and the ground state as an ensemble of ten normal modes. The electron density map is contoured at 3.0 $me^{-}/Å^{3}$, green and red colors indicate higher and lower electron density, respectively, in the non-equilibrium state. The inset shows an overlay of four positions from each of the ten selected normal modes affecting helix 3 around a selected part of the helix, the enhanced mode is highlighted in red. This is the scale of molecular vibrations expected to occur at 297 K. (b) Representation of the normal mode selected to represent the terahertz excited state. The arrows illustrate the eigenvectors of the helix 3 main chain. The inset illustrates the same eigenvectors as seen along the helix direction.

ensemble of all ten modes. The simulated excited states and ground state were then used in a calculation of ten difference electron density maps, one map per mode (see "Material and Methods" section for details). Some maps (but not all) give positive electron density features around helix3, but especially one of these maps displays positive electron density similarly to what was observed in the difference map obtained in our experiment (Fig. 1), and is shown in Fig. 4(a). By the similarity in electron density between the simulated map and the experimental map, we get an indication on which of the modes best represents the vibrational mode of the Fröhlich condensate formed in our experiment. The mode representing the excited state is shown in Fig. 4(b) and the motion of the mode can be described as a composite twist and longitudinal breathing motion in helix 3. In this normal mode analysis, the compatibility between Fröhlich model and the observed positive electron increase has been demonstrated.

To gain insight into how frequently terahertz photons can excite molecular vibrations, we estimated the power absorbed by the crystal in our experimental setup (more details in "Materials and Methods" section). From the estimated terahertz absorption and the number of molecules in the probed crystal volume, we estimate that there is one 0.4 THz photon absorbed per lysozyme molecule in 1 ms (see more details in Materials and Methods section). Accordingly, even if the absorption of every terahertz photon lead to structural changes, a lifetime of $\sim$25 μs is required to maintain a $\sim$10% excited population which would be needed for detection in our experiment.

What is the origin of the long lifetime of the excited state? One possible cause would be that the induced molecular vibrations are underdamped. But while underdamped low frequency vibrations are commonly observed in proteins and their chromophores,[5,12–15] underdamping at 0.4 THz would produce a lifetime in the ns range so this mechanism alone would not explain the microsecond-to-millisecond lifetime of the terahertz radiation induced structural changes observed in the protein crystal studied here. Fröhlich's condensation model,[6] on the other hand, provides a theoretical framework on how vibrational excitation from multiple terahertz photons is stored for an extended period of time, and given all arguments and considerations above we conclude that Fröhlich condensation is the most plausible explanation for our results.

Conclusions

The most important result of this study is that the observed electron density changes in the protein can be unambiguously explained by the absorption of terahertz radiation. According to our analysis, the observed electron density changes can only be explained by a collective excitation of dipole oscillators in the protein as envisaged by Fröhlich. The presence of collective vibrational excitation in biomolecules gives extensive consequences on the self-organization within cells and on the non-equilibrium thermodynamics of reactions involving protein molecules. For example, different intensities of terahertz radiation may alter the Boltzmann factor between vibrational states, making the protein reaction rates dependent on the terahertz radiation drive rather than the temperature in thermal equilibrium. Hence, in living organisms, collective excitation can act as a fundamentally physical rather than biochemical regulatory mechanism.

MATERIALS AND METHODS

Crystallization and X-ray data collection

Tetragonal lysozyme crystals were grown with the hanging drop vapor diffusion method. Lyophilized chicken egg white lysozyme was provided by Sigma-Aldrich (St Louis, MO) and used without further purification. The protein was dissolved in 50 mM sodium acetate, pH 4.5, to final concentrations ranging from 30 to 100 mg/ml. A precipitant solution of 1 M sodium chloride and 25% (v/v) ethylene glycol in the same buffer were used. The hanging drop contained 1 μl or 2 μl protein solution mixed with 1 μl precipitant solution and was set up over a reservoir of 500 μl precipitant solution. Crystals were appearing within 1–3 days and had dimensions of 0.1–0.6 mm.

Lysozyme crystals were mounted on a micro loop bent 90° to the spindle axis with a minimum amount of liquid. We used the diffractometer at beamline P14 (PetraIII) which has a vertical spindle in a hanging configuration. The mounted crystal was protected from drying out with a room temperature capillary (MiTeGen, Ithaca, NY) sealed with vacuum grease. A 297 K nitrogen gas stream was directed close to the crystal at a flow of 10 l/min to ensure a stable temperature. Prior to data collection, the crystal was positioned so that the normal of one of the large crystal faces was aligned with the rotation axis according to Fig. S3(b).[10] We collected extremely fine sliced (0.01°/frame) X-ray diffraction data from tetragonal hen-egg white lysozyme crystals in shutterless (continuous X-ray exposure) mode using 40 Hz readout frequency on a Pilatus 2M-F detector. The detector recorded each diffraction image for 20 ms and 5 ms was spent with readout. The experimental arrangement is illustrated in Fig. S3.[10] The crystals were illuminated by a purpose built amplifier multiplier chain pumped by a built in PDRO source (Viginia Diodes Inc., Charlottesville, VA) capable of delivering 390.4 GHz radiation at total power of 12 mW. The THz source was illuminating the crystals for 25 ms in every second X-ray detector readout cycle starting with a cycle with no terahertz illumination. In total, diffraction data was recorded from seven crystals on 142 500 diffraction frames with 0.4 THz radiation. A reference data set was also collected with the terahertz source switched off during collection of all diffraction images and the data were then divided into two groups depending on the parity of the image sequence number (odd and even). Even (THz on) and odd (THz off) frames were pooled and processed separately. Merged diffraction data and refinement statistics processed to 1.7 Å resolution for the terahertz experiment are summarized in Table I and the control experiment in Table S2.[10] Despite the unconventional data collection strategy, the data quality is very high [I/σ 75.6 (10.5), $CC_{1/2}$ 100.0 (99.1)] and the resolution is limited by the detector distance constraints imposed by the insertion of the terahertz radiation source. When comparing the THz_{on} and THz_{off} merged datasets not only the processing quality indicators (R_{merge}, I/sigma, $CC_{1/2}$) are very similar but also the indexed unit cell dimensions also agree extremely well (deviation between a THz_{on} and THz_{off} dataset obtained from the same data collection is less than 0.001 Å) suggesting that systematic errors between reticular datasets are very similar and the terahertz radiation do not induce major changes in the crystal structure. The scaling R factor between the THz_{on} and THz_{off} data sets is 0.8% at 0.4 THz significantly less than the typical crystallographic modelling error at this resolution (R_{free} close to 20%), but more than what is present between the odd and even images of the reference data set where the terahertz radiation is switched off for both the odd and even frames (0.7%) (Table S2).[10] The X-ray beam with a wavelength of 0.70295 Å (17.638 keV) was defocused to 20 μm in the horizontal direction and shaped with slits to 10 μm in the vertical direction (no focusing). 2% of the total transmitted beam was used (approximately 3×10^9 photons/s). The image to image absorption difference is expected to be 67.5 Gy and this difference is present between integrated datasets of odd and even frames.[16] The X-ray beam was offset from the spindle axis by approximately 50 μm leading to a reduced total absorption of the exposed volume. The central panels of Pilatus 6 M detector were only used and the detector was placed at 280 mm from the crystal.

X-ray crystallographic data analysis

X-ray diffraction images were integrated and scaled using the XDS package.[17] Difference Fourier maps were calculated using components from the CCP4 package.[18] The terahertz radiated and ground state structure factor amplitudes were scaled together with the program SCALEIT.[19] The phases were based on a ground state refined model of lysozyme and calculated by the program SFALL.[20] Difference in amplitudes were weighted by the sigmaA coefficient calculated by the program SIGMAA of the CCP4 package.[21] The scaling of datasets and map calculations were performed within CCP4.[22] Refinement of the crystallographic model was carried out by REFMAC5.[23]

The difference in B-factors were calculated from models refined against diffraction data from the separated even and odd frames of the 0.4 THz and reference data. The longitudinal coordinate shifts along helix 3 were calculated using the same. A singular value decomposition

was performed on the backbone atom coordinates of residues 90–100 of helix 3 giving the longitudinal helix vector as the first principal component. A vector was defined for each atom in the full helix from an arbitrary point outside the helix and was then projected onto the longitudinal axis.

Estimation of temperature change in the crystal

The temperature change induced by 0.4 THz illumination was monitored by an Optris PI 450 infrared camera (Optris, Berlin, Germany) with 40 mK temperature and 12.5 ms time resolution. During the crystal temperature measurements, the lysozyme crystals were dipped in perfluoropolyether oil (Hampton Research, Aliso Viejo, CA) to prevent drying instead of using the capillary as in the diffraction experiment since a thermal image of the crystal cannot be recorded using a capillary. Then the crystals were mounted freely in a Mylar loop while the opening of the horn antenna was positioned at 3 mm from the crystal. The crystals were repeatedly exposed to terahertz radiation for 28 s and allowed to cool down for 28 s. During this measurement no temperature control (gas flow) was employed. A typical thermal image without emissivity calibration is displayed in Fig. 5(a) and the temperature of the probed area as a function of time is shown in Fig. 5(b). In the investigated time frame the crystals reproducibly heated and cooled as a response to the illumination protocol. For oil covered crystals the average rate of temperature increase is 0.10 ± 0.01 K/s. Similarly, cooling rate was calculated to be 0.10 ± 0.03 K/s. After 5.00 ± 0.93 s the temperature reached a steady state at approximately 0.65 ± 0.10 K higher compared to the starting reference temperature. From the rate of the temperature increase, we estimate that at the end of a 25 ms terahertz exposure the crystal has been heated up by 2.6 mK. Out of these 25 ms only 20 ms are probed by X-rays in the diffraction experiment yielding an average crystal temperature increase of 1.0 mK per diffraction image. The average temperature increase is likely to be less in the experimental setup used at X-ray

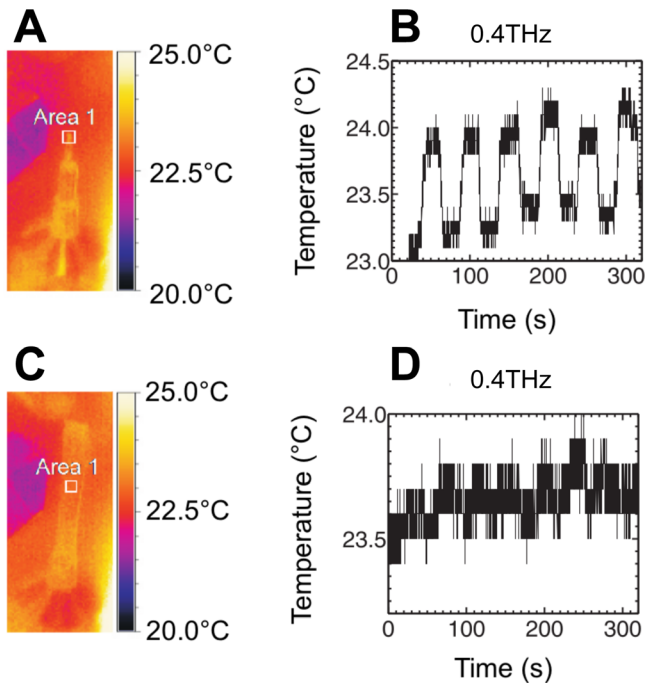

FIG. 5. Measurement of temperature change upon irradiation. (a) Thermal image without emissivity correction of oil covered lysozyme crystal mounted in a Mylar loop. (b) Temperature fluctuation monitored in these freely mounted crystals when illuminated by 0.4 THz radiation in 56 s periods with a duty cycle of 50%. (c) Thermal image without emissivity correction taken of a capillary covered lysozyme crystal while a temperature controlled nitrogen gas flow is applied. (d) Temperature change over time when a crystal covered with capillary is illuminated with 0.4 THz radiation in 56 s periods with a duty cycle of 50%.

data collection (Fig. S1)[10] when a dry N_2 gas stream (10 l/min, 297 K) was continuously blowing on the sample. In this case, temperature fluctuations are hardly visible for 0.4 THz which may be partly due to the capillary concealing the crystal (Fig. 5(d)).

Estimation of the absorbed power

In order to study the effect that the capillary has in the radiation beam, COMSOL Multiphysics simulations were performed. In the simulations the crystal was approximated as a water sphere of 150 μm radius located inside a 2 mm radius capillary 25 μm thick. As in the experimental case, the capillary and the terahertz beam form a 55° angle. The crystal is located at 3 mm from the opening of the antenna which is radiating as a Gaussian (84% of the power) at 0.4 THz. As can be observed in Fig. S4,[10] the small thickness of the capillary compared to the wavelength results in a minimal diffraction so the capillary can be neglected.

For the estimation of the absorbed power, the lysozyme crystal was approximated as water with an absorption coefficient of 150 cm^{-1} and a refractive index of 2.4 for 0.4 THz (Ref. 24) and the capillary was not considered due to the low influence observed in the simulations. The terahertz source provides 12 mW power, 84% of which is concentrated in a Gaussian beam. Considering the Gaussian part of the radiation and the antenna specifications of the source, the power density of the wavefront 3 mm away from the antenna (location of the crystal during the experiment) is around 78 mW/cm^2. The interface between the air and the crystal reflects 22% of the power so the power that reaches the crystal is 62 mW/cm^2. A typical sized crystal (with cubic approximation 300 μm × 300 μm × 300 μm) absorbs 55 μW of which approximately 29 μW absorbed already in the outermost 50 μm layer of the crystal. In this region of the crystal, the absorbed power density is approximately 120 kW/mol of crystalline lysozyme molecule.

Considering the dimensions of the unit cell of the lysozyme crystal (79 Å × 79 Å × 38 Å), the number of 0.4 THz photons that enter each unit cell per millisecond is around 6.8×10^4. In order to roughly estimate the number of photons absorbed per molecule and millisecond, we approximate once more the protein crystal to water with absorption coefficient of 150 cm^{-1}. The energy absorbed by each unit cell is $\frac{E}{n} = \frac{t*V_{unit}*(1-e^{-\alpha l})D}{l}$, where t is exposure time, V_{unit} is the volume of the unit cell, α is the absorption coefficient, D is the power density, and l is the depth of the surface layer. With these approximations, around eight photons are absorbed in each unit cell per millisecond. Considering that each unit cell has eight molecules, we estimate that there is one photon absorbed per lysozyme molecule during 1 ms.

Normal mode analysis

Full-atom normal mode analysis was performed as follows. The lysozyme structure (PDB code 3exd[25]) was downloaded from the protein databank. Protons were added using the Gromacs utility pdb2gmx. Energy minimization was then performed in two steps. First, the Conjugate Gradient algorithm was applied until the maximum force acting on any atom was lower than 10 kJ $mol^{-1} nm^{-1}$. Thereafter, the energy of the system was further minimized by applying the Low-Memory BFGS algorithm. This yielded an energy minimum where the maximal force on any atom was lower than 10^{-9} kJ $mol^{-1} nm^{-1}$. The Hessian matrix of second derivatives of the energy was calculated for the structure at the energy minimum, and normal modes were obtained by diagonalization of the matrix. All calculations were performed in the Gromacs program, version 4.6.5,[26–28] employing the Amber99sb force field.[29] Coulomb and van der Waals interactions were calculated to a cutoff of 1.0 nm employing a shift after 0.8 nm.

Simulated difference Fourier maps

From the 25 modes calculated in the 0.2–0.5 THz range, the ten modes with highest root mean square fluctuation (rmsf) in helix 3 compared to the overall rmsf of the structure were chosen. In this simulation each mode was represented as two harmonic extreme positions of equal populations. In the "ground" state all 20 extreme positions were set to equal occupancy (0.05), whereas in the "excited" state two extreme positions belonging to a single normal mode

were set to 0.5 each and the other modes were omitted. Individual atomic B-factors from the refined model were added, which markedly reduced the influence of large amplitude fluctuation of surface residues. Structure factor amplitudes were calculated up to 1.7 Å resolution and $F_{0.4THz} - F_{off}$ maps were generated using the phases of the ground state structure factors.

ACKNOWLEDGMENTS

X-ray diffraction data was collected at PETRA III beamline P14. Beamtime provisions at beamline 911-3 of Maxlab are also acknowledged. We would like to thank Dr. Thomas Ursby for providing the Bayesian difference Fourier map calculation code and Dr. Sergey Cherednichenko for the help with the testing of the terahertz source. This work was supported by the Swedish Research Council and the Knut and Alice Wallenberg Foundation. X-ray diffraction data and crystallographic coordinates will be deposited in the Protein Data Bank upon acceptance of this manuscript, and released at the date of publication.

[1]N. Go, T. Noguti, and T. Nishikawa, Proc. Natl. Acad. Sci. U. S. A. **80**(12), 3696 (1983).
[2]K. A. Henzler-Wildman, M. Lei, V. Thai, S. J. Kerns, M. Karplus, and D. Kern, Nature **450**(7171), 913 (2007).
[3]M. Karplus, Proc. Natl. Acad. Sci. U. S. A. **107**(17), E71–E72 (2010).
[4]J. Ma, Structure **13**(3), 373 (2005).
[5]D. A. Turton, H. M. Senn, T. Harwood, A. J. Lapthorn, E. M. Ellis, and K. Wynne, Nat. Commun. **5**, 3999 (2014).
[6]H. Fröhlich, Int. J. Quantum Chem. **2**(5), 641 (1968).
[7]P. Weightman, Phys. Biol. **9**(5), 053001 (2012).
[8]J. Pokorny, Bioelectrochem. Bioenerg. **48**(2), 267 (1999).
[9]J. Saint-Blancard, A. Clochard, P. Cozzone, J. Berthou, and P. Jolles, Biochim. Biophys. Acta **491**(1), 354 (1977).
[10]See supplementary material at http://dx.doi.org/10.1063/1.4931825 for additional information about the data collection strategy and validation of the experimental approach.
[11]K. A. Dill, K. Ghosh, and J. D. Schmit, Proc. Natl. Acad. Sci. U. S. A. **108**(44), 17876 (2011).
[12]M. H. Vos, F. Rappaport, J.-C. Lambry, J. Breton, and J.-L. Martin, Nature **363**, 320 (1993).
[13]G. S. Engel, T. R. Calhoun, E. L. Read, T. K. Ahn, T. Mancal, Y. C. Cheng, R. E. Blankenship, and G. R. Fleming, Nature **446**(7137), 782 (2007).
[14]G. Acbas, K. A. Niessen, E. H. Snell, and A. G. Markelz, Nat. Commun. **5**, 3076 (2014).
[15]A. Xie, A. F. van der Meer, and R. H. Austin, Phys. Rev. Lett. **88**(1), 018102 (2002).
[16]K. S. Paithankar, R. L. Owen, and E. F. Garman, J. Synchrotron Radiat. **16**(Pt 2), 152 (2009).
[17]W. Kabsch, Acta Crystallogr. D **66**(Pt 2), 125 (2010).
[18]Collaborative Computational Project Number 4, Acta. Crystallogr. D **50**(Pt 5), 760 (1994).
[19]L. Howell and D. Smith, J. Appl. Cryst. **25**, 81 (1992).
[20]R. C. Agarwal, Acta Crystallogr. A **34**, 791 (1978).
[21]R. J. Read, Acta Crystallogr. A **42**(pt.3), 140 (1986).
[22]M. D. Winn, C. C. Ballard, K. D. Cowtan, E. J. Dodson, P. Emsley, P. R. Evans, R. M. Keegan, E. B. Krissinel, A. G. W. Leslie, A. McCoy, S. J. McNicholas, G. N. Murshudov, N. S. Pannu, E. A. Potterton, H. R. Powell, R. J. Read, A. Vagin, and K. S. Wilson, Acta Crystallogr. Sec. D: Biol. Crystallogr. **67**(Pt. 4), 235–242 (2011).
[23]G. N. Murshudov, P. Skubak, A. A. Lebedev, N. S. Pannu, R. A. Steiner, R. A. Nicholls, M. D. Winn, F. Long, and A. A. Vagin, Acta Crystallogr. D **67**, 355 (2011).
[24]P. H. Siegel, IEEE Trans. Microwave Theory **52**(10), 2438 (2004).
[25]B. G. Guimaraes, L. Sanfelici, R. T. Neuenschwander, F. Rodrigues, W. C. Grizolli, M. A. Raulik, J. R. Piton, B. C. Meyer, A. S. Nascimento, and I. Polikarpov, J. Synchrotron Radiat. **16**(Pt 1), 69 (2009).
[26]D. Van Der Spoel, E. Lindahl, B. Hess, G. Groenhof, A. E. Mark, and H. J. Berendsen, J. Comput. Chem. **26**(16), 1701 (2005).
[27]H. J. C. Berendsen, D. Vanderspoel, and R. Vandrunen, Comput. Phys. Commun. **91**(1–3), 43 (1995).
[28]B. Hess, C. Kutzner, D. van der Spoel, and E. Lindahl, J. Chem. Theory Comput. **4**(3), 435 (2008).
[29]V. Hornak, R. Abel, A. Okur, B. Strockbine, A. Roitberg, and C. Simmerling, Proteins **65**(3), 712 (2006).